Research Article BEU Fen Bilimleri Dergisi 15(1): 492-505 (2026) DOI: 10.17798/bitlisfen.1841878

BİTLİS EREN UNIVERSITY
FEN BİLİMLERİ DERGİSİ
ISSN: 2147-3129 / e-ISSN: 2147-3188

EVALUATING METEOROLOGICAL EFFECTS ON WIND TURBINE PERFORMANCE: ANOMALY ANALYSIS AND ENERGY LOSS QUANTIFICATION

Gökhan YÜKSEK

Batman University, Electrical and Electronics Engineering Department, Batman, Türkiye, gokhan.yuksek@batman.edu.tr

Article Info

Received: *December 14, 2025*
Revised: *February 2, 2026*
Accepted: *February 24, 2026*

Keywords

Wind turbine performance,
Power curve anomaly detection,
Energy loss quantification,
Atmospheric effects,
Wind energy assessment,
Operational data analysis

ABSTRACT

This study investigates how ordinary atmospheric conditions induce systematic deviations from the nominal manufacturer's power curve of a modern wind turbine using a residual-based comparative power curve analysis. The approach directly compares theoretical power values with turbine-level SCADA measurements. It evaluates the difference between predicted and measured power as a continuous indicator of relative underperformance rather than as a classified anomaly. The dataset comprises wind speed, wind direction, air density, ambient temperature, cloud cover, solar irradiance, and measured electrical power from a Nordex N117/3600 wind turbine over a full annual period, complemented by temporally synchronized atmospheric data. Power residuals are analyzed as functions of wind speed and paired meteorological variables to reveal recurring deviation patterns and their physical context. The cumulative integration of positive residuals indicates an annual energy production loss of approximately 244,481 kWh, demonstrating that small but persistent power-curve departures accumulate into a substantial long-term deficit. The results show that performance deviations concentrate primarily in the partially loaded operating region and are strongly associated with variations in air density and wind regime. At the same time, temperature and radiative variables play a secondary role. The main contribution of this study is the presentation of a physically interpretable, residual-based performance deviation analysis that links power curve departures directly to atmospheric conditions and quantifies their cumulative energy impact without relying on predictive models or formal anomaly detection algorithms.

1. INTRODUCTION

Wind energy is a standard feature of contemporary energy portfolios, yet wind turbines frequently deviate from what their theoretical power curves predict under real operating conditions [1-2]. Manufacturer power curves are defined under standardized and idealized conditions in accordance with IEC 61400-12-1 and therefore represent a normalized reference rather than site-specific operating behaviour [3]. In practice, the atmosphere rarely provides such ideal conditions. As a result, differences between predicted and actual power outputs occur regularly, and these discrepancies point to atmospheric processes that merit closer scrutiny [4].

A turbine is influenced by more than wind speed alone; it operates within a broader meteorological environment. Variations in wind direction, temperature, air density, cloud cover, and incoming solar irradiance all contribute to modifying the kinetic energy available at the rotor [5-6] How these influences combine is rarely predictable, and the concept of a single power curve captures only a limited portion of this complexity. When atmospheric conditions depart from the assumptions embedded in the theoretical curve, production may vary in ways that remain hidden if only nominal characteristics are considered [7]. This naturally raises the question of when and under what conditions a turbine departs from its expected operating region.

While previous studies have addressed parts of this problem, analyses are often restricted to a small subset of meteorological variables and/or simplified operating scenarios. Many works apply anomaly detection techniques without explicitly associating detected deviations with the concurrent atmospheric states that give rise to them, which limits interpretability [8-10]. Recent datasets and high-frequency SCADA records now allow turbines to be studied in far greater detail [11-12]. Yet many analyses still treat environmental drivers as background noise rather than active components of performance change, even when advanced machine learning and deep learning techniques are employed [13-15]. Approaches that integrate physical reasoning with empirical evidence, therefore, remain limited, despite their importance for explaining how persistent, small deviations accumulate into measurable energy losses [16-19]. Integrating these complementary viewpoints offers a way to move beyond broad correlations and toward a clearer picture of how atmospheric states shape day-to-day efficiency. This study adopts that view and uses it to connect observed departures from the power curve with the meteorological conditions that give rise to them.

Previous work on power-curve deviation and performance calculation for wind turbines has mostly relied on one of the following methods: prediction-based modeling, statistical anomaly detection, or machine-learning-based classification. Likewise, in many cases, deviations are reported as unassociated outliers, not explicitly connected to simultaneously observed atmospheric conditions, and/or not considered from the perspective of cumulative energy loss. In contrast to these studies, the present study is based on a physics-inspired residual formulation that considers theoretical and measured power directly within the power-curve space. Instead of introducing a new predictive model or detection algorithm, the focus is on understanding when and under what meteorological conditions the deviations cluster and on measuring how these common deviations aggregate into annual energy losses.

Accordingly, this work presents a residual-based, operational framework that relates manufacturer-defined power-curve deviations to concurrent atmospheric conditions and integrates them into a time-resolved estimate of energy loss over the full annual period. The analysis is conducted using on-site SCADA data from a Nordex N117/3600 wind turbine for 2018, together with temporally synchronized meteorological fields from NASA MERRA-2. The main contributions include: (i) a consistent residual definition for theoretical-versus-measured power across the complete record, (ii) two-dimensional loss maps under paired atmospheric variables, and (iii) an annual loss quantification derived from the integrated power deficit.

2. DATASET AND THEORETICAL BACKGROUND

This study is based on operational data collected from a Nordex N117/3600 wind turbine located in Yalova, Turkey (latitude 40.59528°, longitude 28.99035°). The primary dataset spans the full calendar year of 2018 and was obtained from the turbine's Supervisory Control and Data Acquisition (SCADA) system via an open-access repository [20-21]. In addition to turbine-operational measurements, the dataset includes manufacturer-provided theoretical power-curve values.

Turbine information is summarized below to provide context for the operating regime. The analyzed unit is a turbine with a rated power of 3.6 MW and a rotor diameter of 117 m. The turbine operates between the manufacturer-defined cut-in and cut-out wind speeds, with a plateau in the rated region typically observed once the inflow reaches the nominal rated wind speed. These specifications provide the physical context for interpreting the partially loaded and rated operating regions discussed in the subsequent power-curve and residual analyses. The SCADA records include hub-height wind speed $v(t)$, wind direction $\theta(t)$, and theoretical power output $P_{\text{theo}}(t)$, measured electrical power $P_{\text{meas}}(t)$, and corresponding time stamps t.

To account for atmospheric influences beyond the turbine-level measurements, the SCADA data were complemented with meteorological variables from NASA's MERRA 2 [22], including air density $\rho(t)$, ambient temperature $T(t)$, precipitation $R(t)$, and cloud cover index $C(t)$. Following temporal alignment, the two data sources were merged into a unified time series defined as

$$\mathcal{D} = \{\mathbf{x}(t_i)\}_{i=1}^{N}, \tag{1}$$

where $\mathbf{x}(t_i) = [v(t_i),\ \theta(t_i),\ \rho(t_i),\ T(t_i),\ R(t_i),\ C(t_i),\ P_{\text{theo}}(t_i),\ P_{\text{meas}}(t_i)]$, and $N = 8760$, corresponding to an hourly resolution over one year.

It should be noted that the NASA MERRA-2 dataset provides meteorological variables at a regional reanalysis scale and is therefore not intended to resolve site-specific micro-topographic effects such as local terrain-induced flow distortion, wake interactions, or fine-scale surface roughness variations at the turbine location. As a result, MERRA-2 data cannot fully capture localised atmospheric features that may influence instantaneous turbine behaviour. In the present study, MERRA-2 variables are used to represent the broader atmospheric background conditions under which the turbine operates, while detailed local flow dynamics remain outside the scope of the analysis.

Because the SCADA measurements were originally recorded at a higher temporal resolution than the meteorological data, the SCADA series was downsampled to an hourly interval. For a generic SCADA variable $s(t)$, the hourly representative value $\bar{s}(t_k)$was computed as

$$\bar{s}(t_k) = \frac{1}{M_k} \sum_{j=1}^{M_k} s(\, t_{k,j}), \tag{2}$$

where M_k denotes the number of high-frequency samples falling within the k-th hourly window. During the merging process, 484 missing hourly entries were identified. These gaps were reconstructed using a hybrid interpolation strategy. Short gaps were filled using a moving average defined as

$$\hat{x}(t_i) = \frac{1}{2L+1} \sum_{j=-L}^{L} x(\, t_{i+j}), \tag{3}$$

while longer gaps were addressed through linear interpolation between neighbouring valid samples,

$$\hat{x}(t_i) = x(t_a) + \frac{t_i - t_a}{t_b - t_a}(x(t_b) - x(t_a)), \tag{4}$$

where t_a and t_b denote the closest preceding and succeeding valid time stamps.

Therefore, the final dataset captures the full spectrum of seasonal operating conditions for the turbine throughout the year. Figure 1 is an exploratory diagnostic view of the multivariate data structure. The diagonal panels show the empirical distributions for each variable, and the scatter plots in the lower triangle show the bivariate relations, revealing both structured dependencies and more diffuse patterns. The linear correlation coefficients (above the triangular panel) are dominated by wind speed for both theoretical and measured power output. The weaker correlations for parameters such as cloud cover, precipitation, and solar irradiance suggest that these have a less direct effect on turbine efficiency. Taken together, these visualizations provide a better understanding of the dataset's internal structure for more granular analysis.

The correlation coefficients between the parameters and the physical phenomena underlying wind energy production support one another, so one must be convinced of their existence to understand what the dataset expresses. Factors such as wind speed, wind direction, air temperature, and cloud cover play a critical role in energy production estimates, and each variable naturally affects energy production. Wind speed is one of the most essential variables for wind energy production, with a correlation coefficient of 0.97. Wind turbines convert the wind's kinetic energy into electrical power, with output governed by

$$P = \frac{1}{2} \cdot \rho \cdot A \cdot v^3 \cdot C_P \tag{5}$$

here, ρ is air density, A is the swept area of blades, v is wind speed, and C_P is the turbine's efficiency. A detailed explanation is given in Table 1. Since power increases with the cube of wind speed (v^3), even

small wind speed changes significantly impact energy production. However, turbines operate efficiently only within specific wind speed ranges, balancing energy output and mechanical safety, with efficiency limited by Betz's law to about 59.3% [23-24].

Table 1 Wind turbine output formula ingredients

Variable	Mathematical Relation	Explanation
Wind Speed (v)	$P \propto v^3$	Wind power scales with the cube of wind speed because the kinetic energy flux increases sharply as velocity rises.
Air Density (ρ)	$P \propto \rho$	Higher air density increases the mass flow through the rotor, boosting available kinetic energy and enhancing power generation.
Swept Area (A)	$P \propto A$	A larger rotor area interacts with a greater volume of moving air, allowing the turbine to extract more energy from the wind.
Wind Direction	Logical relationship with C_p	When the wind approaches the rotor at a favorable angle, the power coefficient improves; deviations from this angle reduce aerodynamic efficiency.
Temperature (T)	$P \propto \frac{1}{T}$ via ρ	Lower temperatures increase air density, which in turn increases power output.
Cloud Cover	Logical relationship with solar irradiation and wind speed	Cloud cover can influence atmospheric stability and local wind behavior; in hybrid systems, it also affects the solar resource.
Prectotland	Potential relationship with wind conditions	Heavy precipitation may disrupt wind patterns and turbine efficiency.

When analyzing wind turbines, one of the first considerations is the range of wind speeds in which they can operate reliably. Turbines also respond differently to shifts in wind direction, since each machine is designed around a preferred inflow angle. Sudden changes in direction or persistent misalignment can reduce usable energy, and these effects often appear in long-term production records. The predictability of such a system, therefore, hinges not only on routinely measured variables but also on irregular or locally driven influences. Forecasting methods must account for these distortions, or suppress their effects when needed, particularly in landscapes where terrain or built structures deflect the flow [25].

Temperature also affects the power equation, but it is not directly included in it. Its primary effect is to change air density, which decreases with increasing temperature. In principle, this relationship is straightforward, but in practice, humidity and pressure complicate matters. Cold, dense air helps the turbine generally extract more energy, while hot weather conditions reduce output. High temperatures also shorten component lifespans and can lead to more frequent maintenance. Other atmospheric variables also come into play. Cloud cover, atmospheric stability, and wind restrictions during weather fronts will also affect production. At times, the impact is slow and steady and difficult to discern. At other times, these effects occur abruptly, leading to a noticeable drop in output [26].

The pairplot provides a summary of the relationships among the variables in the dataset, including both empirical and theoretical power outputs. Several patterns stand out. In the bottom-right elements of the matrix, the strongest convergence is observed among Wind Speed, LV Active Power, and the theoretical power curve. Wind Speed exhibits an almost linear relationship with the theoretical curve and a capacity-limited relationship with LV Active Power, which is typical for a turbine power curve. Correlation values of 0.93–0.97 further emphasize the importance of wind speed.

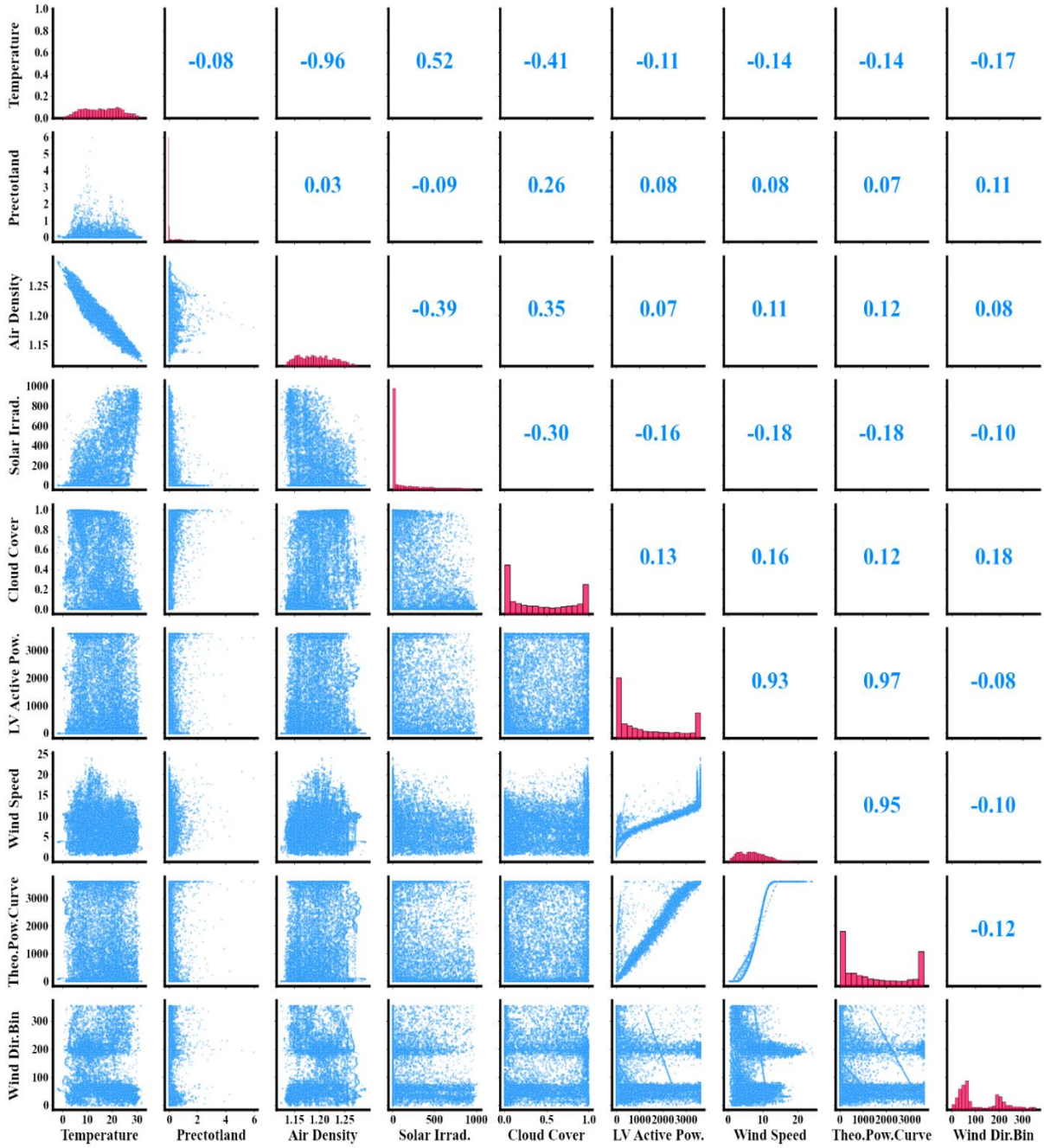

Figure 1 Plot set showing the relationships between variables in the dataset

The diagonal histograms further confirm this view: Wind Speed is right-skewed, and LV Power is concentrated at low speeds and flattens out at rated production. Temperature and humidity have a more modest effect on power output. Air density is associated with power in the mid-range, with correlation coefficients ranging from 0.35 to 0.40, reflecting its physical role. Scatter plots show that denser air shifts the power curve upward. There is no correlation between cloud cover and rain, suggesting that these variables do not affect the results in this dataset. Solar irradiance shows essentially no correlation with wind-related variables, consistent with expectations given the independence of solar and wind resources at this site. Wind Direction is the weakest correlate overall and is believed to add little beyond what is already explained by wind speed.

Overall, the matrix forms a coherent physical picture: wind speed governs production, air density modulates it slightly, and most other meteorological variables exert little direct influence. This structure ensures that the dataset behaves as expected and provides a solid basis for later modelling and variable selection.

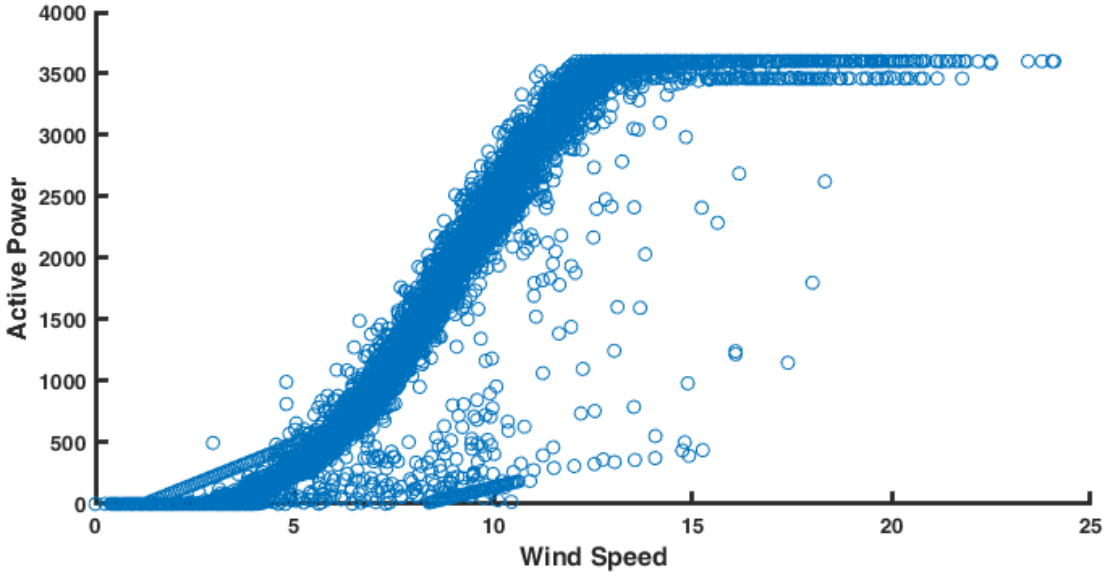

Figure 2 Actual turbine active power plotted against wind speed, showing the characteristic power-curve pattern

Figure 2 offers a clear view of how wind speed relates to active power. At the low end of the scale, the turbine produces very little energy; the dense cloud of points below about 4 m/s reflects operation before the machine reaches its cut-in threshold. Once the wind climbs into the 5–9 m/s range, the picture changes quickly. Power output rises in a steep, well-defined band that mirrors the linear section of a typical turbine power curve, and the tight clustering in this region points to stable aerodynamic behavior.

As wind speed approaches 10–12 m/s, the curve flattens. The turbine is near its rated capacity, and pitch control begins to limit the aerodynamic load, creating the horizontal plateau in the plot. The broader scatter within this zone is not unusual; turbulence, brief changes in inflow, or the timing of the control system can all cause small variations around the nominal output. Taken as a whole, the plot reproduces the familiar turbine power curve and provides an additional check on the dataset's coherence.

Figure 3 shows a polar scatter plot of wind direction versus LV active power, allowing the variation in output to be seen around the full circle. The cluster of points between about 20° and 80° stands out right away. Winds from this northeast corridor are prevalent and productive, and the turbine typically produces more power in this sector. A broader spread of points in this area indicates that a small variation in wind speed or turbulence intensity will cause a different response of the turbine. Even if the direction of the incoming wind remains fairly steady, power generation can still rise and fall due to changing local flow conditions. This behaviour is typical of turbulent inflow and indicates that power fluctuations are not solely due to wind direction. From 200° to 260°, another pattern emerges. There are fewer points in this area, and they are mostly linked with the lowest power values. The southwest winds are less frequent and tend to provide less useful power. This can be due to lower average wind speeds or to wake effects produced by surrounding terrain or upwind obstacles. Around 180°, the long, narrow bands are associated with extremely long, weak wind sequences, with the turbine still running but far from its nominal output. The directional distribution, therefore, suggests that wind speed is not uniform in all directions. Power generation is concentrated in distinct angles, which makes the pattern slightly squashed or elliptical. This directional preference reveals interesting local wind features. It also indicates that possible gains in matching performance may be attained by evaluating yaw behaviour and tuning directional control.

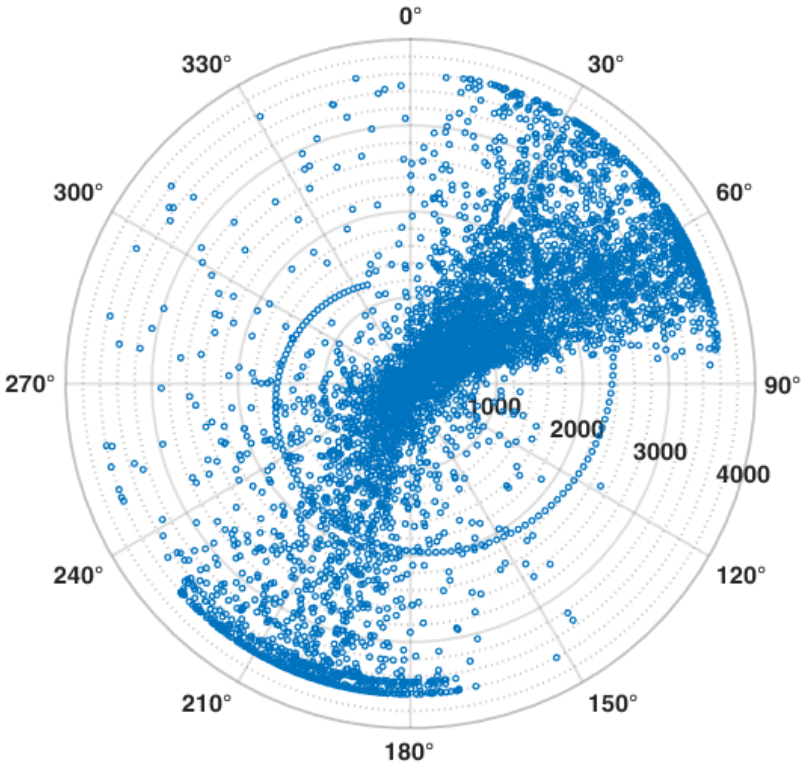

Figure 3 Polar scatter plot showing the distribution of active power as a function of wind direction

All data processing, analysis, and visualization steps in this study were performed using Python in an offline post-processing environment. Numerical operations and data handling were performed with standard scientific computing libraries, and all figures and plots were generated programmatically to ensure consistency and reproducibility. No real-time control or embedded implementation was used; the analysis was conducted entirely on archived SCADA and meteorological datasets.

3. ANOMALY ANALYSIS

In this study, the term "anomaly" is used in a descriptive and operational sense rather than as the outcome of a formal classification or detection algorithm. Deviations from the theoretical power curve are interpreted as relative performance deviations with respect to an idealized reference curve, rather than as absolute measures of site-specific turbine efficiency. Anomalies are therefore defined as sustained positive residuals between the manufacturer-provided theoretical power curve and the measured turbine output, indicating periods of relative underperformance under comparable wind conditions. No fixed statistical threshold or machine-learning-based classifier is imposed; instead, the residual time series is examined directly to characterize when and under which atmospheric conditions these deviations systematically occur.

It is important to emphasize that the present analysis does not aim to classify operating points into discrete normal or anomalous states using predefined thresholds or statistical decision boundaries. The reported residual magnitudes are therefore not interpreted within a formal classification framework. Instead, they are treated as continuous indicators of deviation from the theoretical power curve, used to examine relative underperformance patterns and their cumulative impact on energy production. Accordingly, the terminology employed throughout the study reflects a descriptive deviation analysis rather than a threshold-based or data-driven anomaly detection scheme.

Figure 4 plots the measured power output alongside the theoretical curve and shows where the turbine follows the expected response and where it begins to deviate. At low wind speeds below 4–5 m/s, agreement is generally good, as aerodynamic loading is weak and the turbine output remains close to the reference curve, with only small deviations. As wind speed moves into the mid-range, around 6–12 m/s, the spread of measured points increases, and many values fall below the ideal curve. In this region,

the turbine becomes more sensitive to turbulence, small yaw misalignments, and changes in air density, which reduce efficiency and lead to noticeable underperformance.

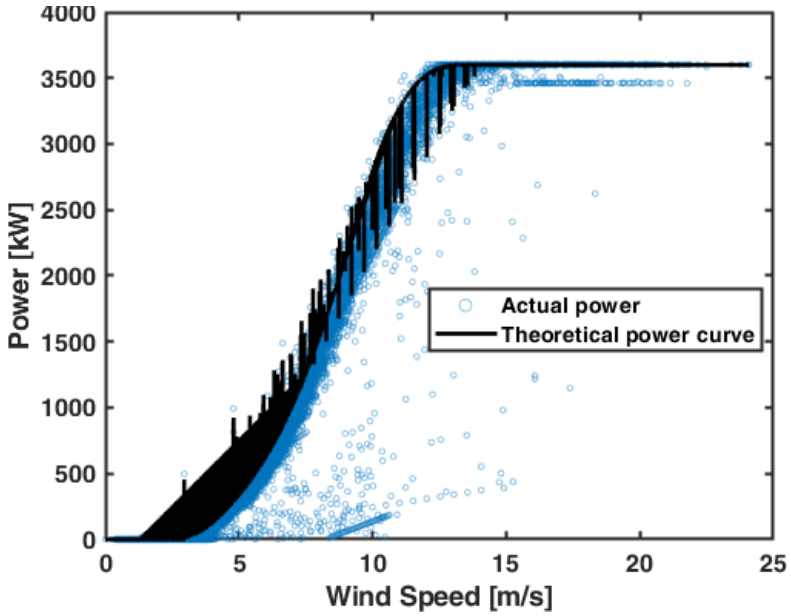

Figure 4 The theoretical and measured turbine power curves plotted against wind speed

Closer to the rated region, approximately 11–14 m/s, the theoretical curve begins to level off, while the measured output does not follow this transition as smoothly. Periods of reduced power continue to occur, indicating intervals during which pitch or torque control does not fully maintain optimal energy capture. At higher wind speeds, approaching 20–25 m/s, the gap between theoretical and measured outputs narrows again as both converge toward rated power and are constrained by the turbine's protection mechanisms. Taken as a whole, the increasing divergence between the ideal and observed values in the mid-to-upper wind speed range reflects recurrent power-curve deviations. These deviations constitute the residual basis for subsequent analyses and help explain the cumulative energy losses discussed in later sections.

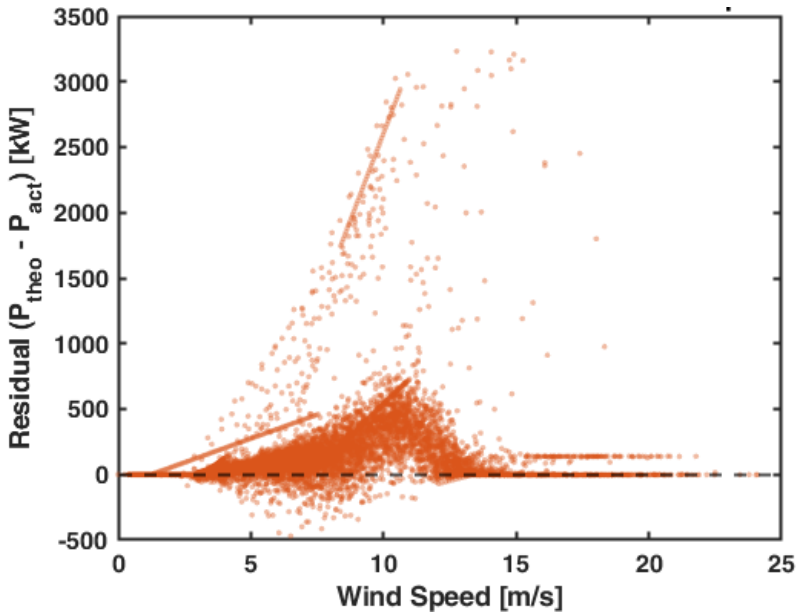

Figure 5 Residual deviations between theoretical and actual power values as a function of wind speed

Figure 5 shows how residuals vary with wind speed and clearly identifies where the turbine deviates from the expected curve. At low speeds (<4 m/s), residuals remain close to zero, indicating that the measured output closely follows the theoretical estimate. As wind speed moves into the 6–12 m/s range, residuals increase and scatter. A dense band of positive values emerges, often linked to turbulence, higher aerodynamic loading, or minor yaw errors that reduce efficiency. The most pronounced deviations occur between about 8 and 14 m/s. Residuals in this band can reach 500–1500 kW, with some exceeding 2500 kW. These large gaps indicate periods when the turbine underperforms its expected output. Pitch-control actions, density assumptions, or brief derating events may all play a role. Above about 14 m/s, residuals contract again. Both the theoretical and measured outputs level off at rated power, and the differences shrink toward zero. This pattern shows that most efficiency-related departures occur not at the extremes but in the partially loaded part of the curve, where aerodynamic and control factors interact most strongly. Overall, the wind-speed-based residual plot narrows the problem to the 6–14 m/s band, the zone where most energy losses accumulate and where power-curve anomalies are most frequently generated.

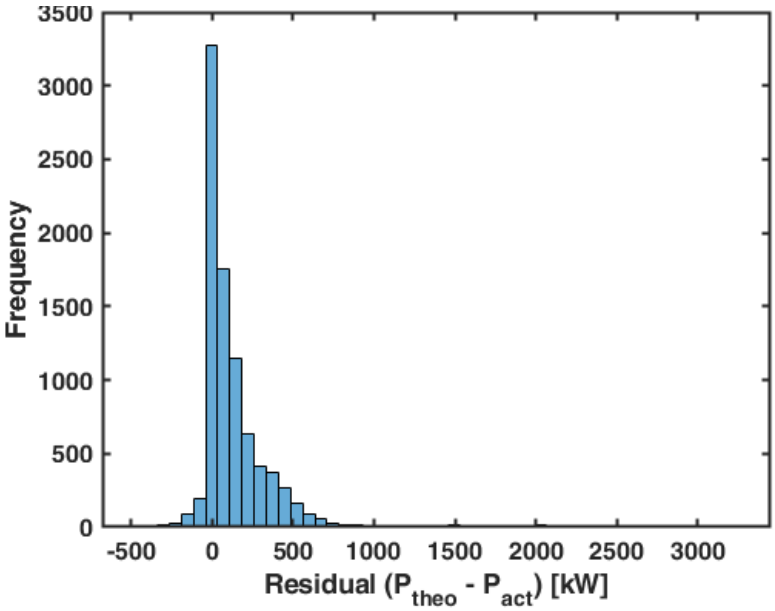

Figure 6 Histogram of power-curve residuals illustrating the distribution of deviations

Figure 6 shows a residual histogram with a clearly uneven shape. Most values cluster near zero, suggesting that many observations represent routine operation in which the measured output does not stray far from the theoretical curve. What stands out, though, is the long positive tail extending beyond 500 kW. These larger residuals correspond to recurring underperformance events hinted at in earlier figures, often tied to aerodynamic limits or control responses that limit power capture. Negative residuals occur only occasionally and remain small.

These events, in which the turbine produces slightly more than expected, usually stem from short-lived advantages such as favorable gusts, measurement noise, or transient turbulence that briefly enhance power capture. Their scarcity indicates that overperformance does not characterize the turbine's overall behavior. The resulting residual distribution is strongly right-skewed, with many values clustered near zero and a long tail toward higher positive deviations. This imbalance indicates a systematic tendency toward energy loss rather than random noise and supports the view that underperformance arises under specific wind and atmospheric conditions. The residual pattern, therefore, provides the statistical basis for subsequent loss quantification and deviation analyses.

It should be acknowledged that the original SCADA measurements were recorded at a higher temporal resolution and subsequently aggregated to an hourly scale to align with the available meteorological data. This temporal averaging inevitably suppresses short-duration effects that are critical to wind turbine aerodynamics, such as turbulence intensity, rapid yaw misalignment, and transient control responses. As a result, the analysis cannot explicitly resolve instantaneous fluctuations that may

contribute to the pronounced residual scatter observed, particularly in the 6–12 m/s wind speed range. Consequently, the elevated residual variability within this band should be interpreted as the cumulative manifestation of unresolved short-term dynamics rather than as a direct representation of individual turbulence events. While higher-resolution SCADA data would be required to explicitly isolate such instantaneous effects, the adopted hourly aggregation remains appropriate for the primary objective of this study, namely the assessment of longer-term performance deviations and their integrated impact on annual energy loss.

4. ENERGY LOSS QUANTIFICATION

To illustrate the temporal evolution of losses, Figures 7 and 8 present a time-series comparison of theoretical and observed turbine power. In Figure 7, the entire operating record is shown, with the theoretical curve exhibiting the expected transitions between the partial-load and rated regimes. At the same time, the measured power displays strong short-term variations around these idealized points. Whenever the actual output is below the theoretical reference, the area is shaded.

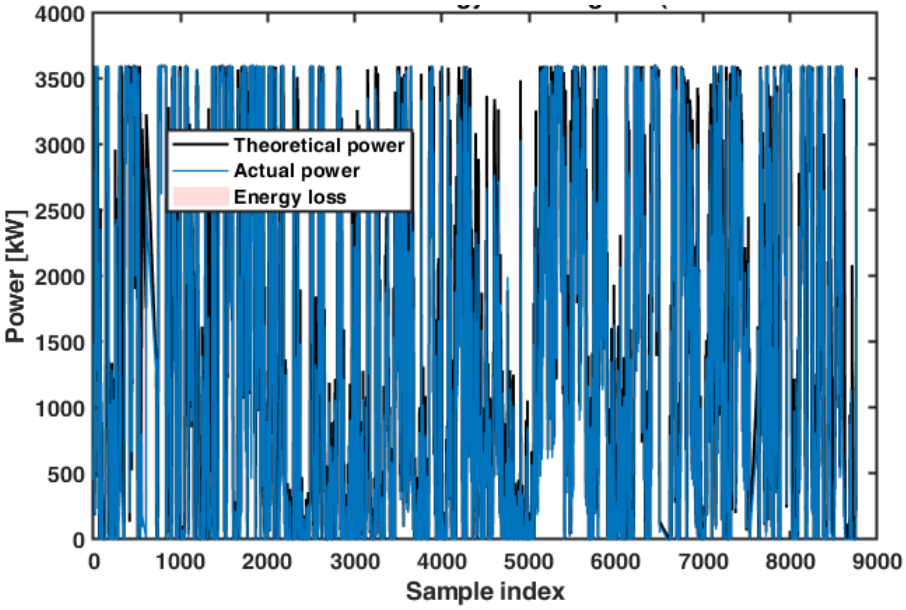

Figure 7 Comparison of theoretical and actual turbine power with highlighted regions of energy loss

These regions represent an instantaneous power deficit. Figure 8 provides an enlarged partial view of Figure 7, highlighting the shaded deficit areas and their temporal arrangement. From the combined figures, it is evident that the overall energy loss is not due to isolated outlier events but rather to small, short-term deficits that accumulate repeatedly during normal operation.

These decrement intervals recur throughout the operating record, indicating that the turbine experiences not a few isolated drops but a recurring pattern of underperformance. Output often alternates rapidly between nominal and lower values, and the shortfalls appear to be mainly associated with rapidly varying atmospheric conditions rather than persistent mechanical faults or systematic curtailment. When integrated over the entire day, such departures from the norm result in energy losses of approximately 244,481 kWh. This loss is not caused by exceptional events but by a slow accumulation of numerous small discrepancies between the expected and measured power, which, taken individually, may seem insignificant but, when aggregated, form a significant annual loss.

Note that certain processes mentioned in the explanation of these losses, including turbulence intensity, yaw misalignment, and fine control actions, were not measured directly in the dataset at hand. Therefore, these terms are used as physically plausible interpretations rather than definitive causal explanations. Consequently, the interpretation of the power loss regimes relies on SCADA and meteorological variables as measured. Still, it acknowledges that unmeasured effects have been inferred and may increase the magnitude and variability of the observed power deficits.

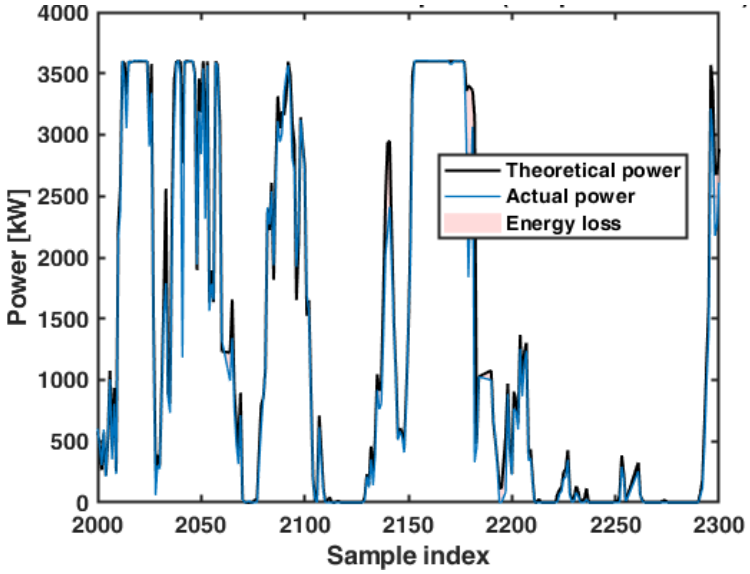

Figure 8 Comparison of theoretical and actual turbine power with highlighted regions of energy loss, zoomed version

The two-dimensional loss map in Figure 9 further illustrates how wind speed and air density jointly influence these deficits. The most prominent loss region appears where density values exceed about 1.26–1.29 kg/m³ and wind speeds fall between 8 and 13 m/s. Under these conditions, the theoretical curve tends to overestimate power, while the real turbine experiences stronger aerodynamic loading and higher turbulence. This produces a cluster of large positive residuals, shown as yellow and green patches on the map.

At lower densities, below roughly 1.22 kg/m³, losses remain small across nearly the entire wind-speed range. The reduced air-mass kinetic energy and the closer match between measured and predicted output keep deviations limited. A similar effect occurs at higher wind speeds, above about 15 m/s, where both theoretical and actual outputs flatten near the rated limit; when the turbine is in saturation, aerodynamic and control constraints override most meteorological influences.

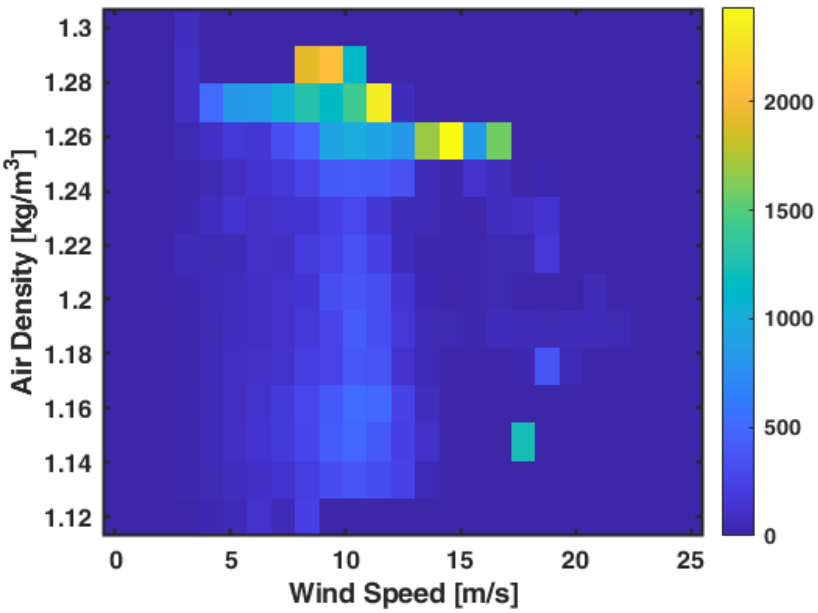

Figure 9 Mean power loss distribution across wind speed and air density conditions

The concentration of losses in the moderate-wind, high-density band underscores the value of incorporating real-time density adjustments into performance evaluation. It also confirms that power-

curve departures are not random but arise under distinct atmospheric conditions. Monitoring strategies that account for these conditions can therefore improve underperformance detection and sharpen future energy-yield estimates.

Figure 10 shows how losses vary with temperature and solar irradiance; unlike patterns tied to wind speed or air density, there is no strong structure here. Across nearly the entire range of temperatures and irradiance levels, the deficits remain modest. A few scattered pockets of higher loss appear at colder conditions, roughly between 0 and 5 °C, combined with moderate irradiance, but these clusters do not form a consistent band or trend. They most likely reflect indirect atmospheric influences, density shifts, or brief turbulence episodes, rather than any direct effect of temperature or sunlight on turbine behavior.

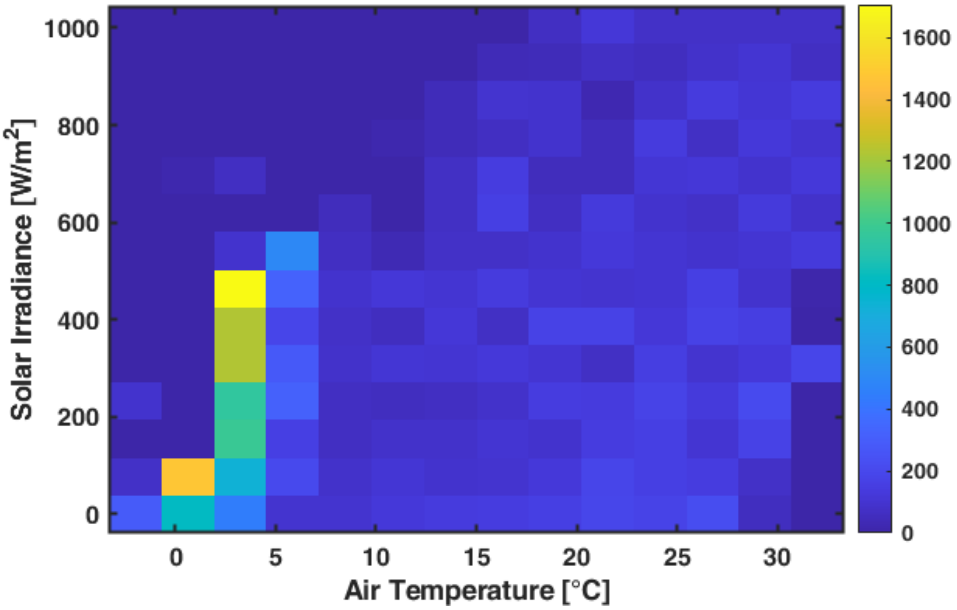

Figure 10 Mean power loss distribution as a function of air temperature and solar irradiance

The lack of a clear high-loss region suggests that temperature and irradiance play only a supporting role in shaping performance. Air density already captures most of the atmosphere's thermal state, and irradiance has no aerodynamic impact on a wind turbine, so their influence is naturally limited. This supports the earlier result that the main drivers of power-curve departures are wind-related variables, especially wind speed and density. At the same time, thermal and radiative factors contribute only in a secondary way.

Taken together, the map aligns with fundamental aerodynamic intuition: turbine output is primarily governed by the kinetic energy of the wind, and other meteorological variables can modify performance only indirectly and to a far lesser extent. Non-wind variables show no strong causal pattern in explaining losses, further confirming that wind-driven mechanisms dominate the deficit dynamics.

This study uses a case-study approach based on measurements from a single wind turbine over a single annual period. Although the dataset is limited to one turbine, it provides a consistent and realistic basis for examining the relationship between atmospheric conditions and power-curve deviations. The objective of this work is to demonstrate the applicability of the proposed residual-based performance-deviation analysis framework under real operating conditions, and to show that it can be readily extended to other turbines and sites in future studies.

5. CONCLUSION

The study's results highlight a familiar but often overlooked reality: a wind turbine's behavior is shaped above all by the atmosphere surrounding it. Among the variables examined, wind speed and air density repeatedly emerge as the dominant factors determining whether the turbine follows its theoretical power curve. Instead of focusing solely on the manufacturer's curve, the analysis compares it directly with the turbine's measured output and identifies gaps between the two. What becomes visible is a consistent

cluster of underperformance in the partially loaded region, the zone where the turbine is not idling but has not yet reached the rating plateau. In addition to reporting annual losses, the study expresses these losses in a joint wind–density condition space, allowing the identification of focal areas of underperformance under typical atmospheric variability.

Residual maps, time-series traces, and loss plots indicate consistent performance. As wind speed approaches the medium range and air density increases, the theoretical power curve begins to overestimate extractable energy. In this case, the turbine experiences higher aerodynamic loading, increased turbulence, and sporadic yaw misalignment, all of which reduce the power output. Other environmental factors, such as temperature, cloud cover, irradiance, and rainfall, have more indirect effects. Their influences are noticeable but insufficient to alter the overall performance trend to the same extent as wind speed and air density.

When aggregated over the year, these relatively small fluctuations add up to a large energy loss of around 244,481 kWh. This loss is not the result of a handful of extreme events but rather of many small excursions during normal operation. This underscores the need to consider meteorological conditions in performance evaluations. Looking at the turbine in isolation from the surrounding atmospheric state masks important signals. An analysis method that accommodates atmospheric fluctuations makes off-nominal conditions detectable earlier and provides a firmer foundation for maintenance scheduling, power-curve surveillance, and operational decision-making.

Acknowledgements

No external financial support was received for this research. This study did not involve human participants, animals, or sensitive personal data; therefore, ethics committee approval was not required.

Statement of Research and Publication Ethics

This study was conducted in accordance with accepted principles of research and publication ethics. All data were used in compliance with relevant data access regulations, and appropriate citation and reporting standards were followed throughout the manuscript.

Artificial Intelligence (AI) Contribution Statement

AI-based language editing tools were used solely for grammar checking and linguistic refinement. No AI tools were used for data acquisition, data preprocessing, analysis, modeling, result interpretation, or figure generation. All scientific content and conclusions were developed exclusively by the author.

REFERENCES

[1] M. C. Alexiadis, P. S. Dokopoulos, H. S. Sahsamanoglou, and I. M. Manousaridis, "Short-term forecasting of wind speed and related electrical power," *Solar Energy*, vol. 63, no. 1, pp. 61–68, Jul. 1998, doi: 10.1016/S0038-092X(98)00032-2.

[2] T. Mahmoud, Z. Y. Dong, and J. Ma, "Advanced method for short-term wind power prediction with multiple observation points using extreme learning machines," *The Journal of Engineering*, vol. 2018, no. 1, pp. 29–38, Jan. 2018, doi: 10.1049/joe.2017.0338.

[3] Nordex SE., "Nordex N117/3600 wind turbine specifications," https://www.nordex-online.com/en/product/n117-3600/.

[4] X. Chen, X. Zhang, M. Dong, L. Huang, Y. Guo, and S. He, "Deep Learning-Based Prediction of Wind Power for Multi-turbines in a Wind Farm," *Front. Energy Res*., vol. 9, Jul. 2021, doi: 10.3389/fenrg.2021.723775.

[5] N. Kirchner-Bossi, G. Kathari, and F. Porté-Agel, "A hybrid physics-based and data-driven model for intra-day and day-ahead wind power forecasting considering a drastically expanded predictor search space," *Appl. Energy*, vol. 367, p. 123375, Aug. 2024, doi: 10.1016/j.apenergy.2024.123375.

[6] Y. Liu, J. Wang, and L. Liu, "Physics-informed reinforcement learning for probabilistic wind power forecasting under extreme events," *Appl. Energy*, vol. 376, p. 124068, Dec. 2024, doi: 10.1016/j.apenergy.2024.124068.

[7] F. Ye, J. Brodie, T. Miles, and A. Aziz Ezzat, "AIRU-WRF: A physics-guided spatio-temporal wind forecasting model and its application to the U.S. Mid Atlantic offshore wind energy areas," *Renew. Energy*, vol. 223, p. 119934, Mar. 2024, doi: 10.1016/j.renene.2023.119934.

[8] E. Zhao, S. Sun, and S. Wang, "New developments in wind energy forecasting with artificial intelligence and big data: a scientometric insight," *Data Science and Management*, vol. 5, no. 2, pp. 84–95, Jun. 2022, doi: 10.1016/j.dsm.2022.05.002.

[9] P. Ekanayake, O. Panahatipola, and J. Jayasinghe, "Development of wind energy prediction models using statistical, machine learning and hybrid techniques: a case study," *J. Natl. Sci. Found*., vol. 50, no. 2, p. 503, Sep. 2022, doi: 10.4038/jnsfsr.v50i2.10591.

[10] M. Li, M. Yang, Y. Yu, and W.-J. Lee, "A Wind Speed Correction Method Based on Modified Hidden Markov Model for Enhancing Wind Power Forecast," *IEEE Trans. Ind. Appl*., vol. 58, no. 1, pp. 656–666, Jan. 2022, doi: 10.1109/TIA.2021.3127145.

[11] K. L. Jorgensen and H. R. Shaker, "Wind Power Forecasting Using Machine Learning: State of the Art, Trends and Challenges," in *2020 IEEE 8th International Conference on Smart Energy Grid Engineering (SEGE), IEEE*, Aug. 2020, pp. 44–50. doi: 10.1109/SEGE49949.2020.9181870.

[12] D. Alves, F. Mendonça, S. S. Mostafa, and F. Morgado-Dias, "The Potential of Machine Learning for Wind Speed and Direction Short-Term Forecasting: A Systematic Review," *Computers*, vol. 12, no. 10, p. 206, Oct. 2023, doi: 10.3390/computers12100206.

[13] Y. Zheng et al., "New ridge regression, artificial neural networks and support vector machine for wind speed prediction," *Advances in Engineering Software*, vol. 179, p. 103426, May 2023, doi: 10.1016/j.advengsoft.2023.103426.

[14] D. Zafirakis, G. Tzanes, and J. K. Kaldellis, "Forecasting of Wind Power Generation with the Use of Artificial Neural Networks and Support Vector Regression Models*," Energy Procedia*, vol. 159, pp. 509–514, Feb. 2019, doi: 10.1016/j.egypro.2018.12.007.

[15] H. Demolli, A. S. Dokuz, A. Ecemis, and M. Gokcek, "Wind power forecasting based on daily wind speed data using machine learning algorithms," *Energy Convers. Manag*., vol. 198, p. 111823, Oct. 2019, doi: 10.1016/j.enconman.2019.111823.

[16] J. Zhang, Z. Zhao, J. Yan, and P. Cheng, "Ultra-Short-Term Wind Power Forecasting Based on CGAN-CNN-LSTM Model Supported by Lidar," *Sensors,* vol. 23, no. 9, p. 4369, Apr. 2023, doi: 10.3390/s23094369.

[17] M. A. A. Al-qaness, A. A. Ewees, A. O. Aseeri, and M. Abd Elaziz, "Wind power forecasting using optimized LSTM by attraction–repulsion optimization algorithm," *Ain Shams Engineering Journal*, vol. 15, no. 12, p. 103150, Dec. 2024, doi: 10.1016/j.asej.2024.103150.

[18] Z. Zhao et al., "Hybrid VMD-CNN-GRU-based model for short-term forecasting of wind power considering spatio-temporal features," *Eng. Appl. Artif. Intell*., vol. 121, p. 105982, May 2023, doi: 10.1016/j.engappai.2023.105982.

[19] Y. Xiao, C. Zou, H. Chi, and R. Fang, "Boosted GRU model for short-term forecasting of wind power with feature-weighted principal component analysis," *Energy*, vol. 267, p. 126503, Mar. 2023, doi: 10.1016/j.energy.2022.126503.

[20] B. Erisen, "Wind Turbine Scada Dataset," https://www.kaggle.com/datasets/berkerisen/wind-turbine-scada-dataset/data.

[21] G. Yüksek, "Optimized GDTP-XGBoost Framework for Wind Power Forecasting Toward Condition-Based Maintenance," Eksploatacja i Niezawodność – *Maintenance and Reliability*, Nov. 2025, doi: 10.17531/ein/214376.

[22] R. Gelaro et al., "The Modern-Era Retrospective Analysis for Research and Applications, Version 2 (MERRA-2)," *J. Clim.*, vol. 30, no. 14, pp. 5419–5454, Jul. 2017, doi: 10.1175/JCLI-D-16-0758.1.

[23] J. F. Manwell, J. G. McGowan, and A. L. Rogers, Wind Energy Explained. Wiley, 2009. doi: 10.1002/9781119994367.

[24] T. Burton, N. Jenkins, D. Sharpe, and E. Bossanyi, Wind Energy Handbook. Wiley, 2011. doi: 10.1002/9781119992714.

[25] J. B. Olson et al., "Improving Wind Energy Forecasting through Numerical Weather Prediction Model Development," *Bull. Am. Meteorol. Soc*., vol. 100, no. 11, pp. 2201–2220, Nov. 2019, doi: 10.1175/BAMS-D-18-0040.1.

[26] M. Rezamand, M. Kordestani, R. Carriveau, D. S.-K. Ting, M. E. Orchard, and M. Saif, "Critical Wind Turbine Components Prognostics: A Comprehensive Review," *IEEE Trans. Instrum. Meas*., vol. 69, no. 12, pp. 9306–9328, Dec. 2020, doi: 10.1109/TIM.2020.3030165.